Document downloaded from:

http://hdl.handle.net/10251/69234

This paper must be cited as:

Portilla Ovejero, MT.; Llopis Alonso, F.; FRANCISCO JAVIER LLOPIS ALONSO; Martínez, C. (2015). Non-oxidative dehydroaromatization of methane:an effective reaction regeneration cyclic operation for catalyst life extension. Catalysis Science and Technology. 5(7):3806-3821. doi:10.1039/C5CY00356C.

The final publication is available at

http://dx.doi.org/10.1039/c5cy00356c

Copyright Royal Society of Chemistry

Additional Information

Non-oxidative dehydroaromatization of methane: an effective reaction-regeneration cyclic operation for catalyst life extension

M. Teresa Portilla[1], Francisco J. Llopis[2], Cristina Martínez[1*]

[1]*Instituto de Tecnología Química (UPV-CSIC), Universidad Politécnica de Valencia-Consejo Superior de Investigaciones Científicas, Av. de los Naranjos s/n, 46022 Valencia, Spain.*

[2]*Departamento de Ingeniería Química, Universitat de Valencia, 46100 Burjassot, Spain*

* Corresponding author: cmsanche@itq.upv.es; Tel.: (34) 963877811, FAX: (34) 963879444

Abstract

Non-oxidative methane aromatization is an attractive direct route for producing higher hydrocarbons, highly selective to benzene despite the low conversions due to thermodynamic limitations, and Mo/H-ZSM-5, the first catalyst proposed for this reaction, is still considered as one of the most adequate. The major problem of this process is the severe catalyst deactivation due to the rapid buildup of carbonaceous deposits on the catalysts.

Here we present an effective regeneration procedure that extends the life of Mo/zeolite based catalysts by combining reaction periods of 1.5 h with 0.5 h regeneration steps in a continuous cyclic mode and methane activation after each regeneration stage. Benzene productivity obtained with Mo/ZSM-5 is shown to be almost constant for increasing TOS ranges when applying this new cyclic protocol, and threefold values are achieved for an 18 h on stream period by limiting the reaction steps to the first 1.5 h of maximum benzene selectivity (97 vs. 33 g benzene/kg cat·h) as compared to a conventional single run.

Key words: methane aromatization, zeolites, Mo/zeolites, deactivation, reaction-regeneration cycles, catalyst life extension

1. Introduction

Methane, the main component of natural gas, is an interesting source of chemicals and clean liquid fuels, and a promising alternative raw material to oil[1-3]. Although conventionally used for electrical power generation and heating, its conversion into higher value products has gained importance along the last decades. On the one hand, the potential reserves of natural gas are larger than the oil reserves, especially if shale gas is considered[4-5], and its composition is very little dependent on the source, and on the other, methane has a high hydrogen to carbon (H/C) ratio. There are different Gas to Liquid (GTL) technologies available to convert this methane by means of indirect or direct processes[6]. At present, all commercially viable processes for methane conversion belong to the group of the so-called indirect routes, where methane is transformed into the more reactive synthesis gas mixture ($CO+H_2$, also named as syngas). After this first step, syngas can be later converted into hydrocarbons or higher alcohols by means of the Fischer-Tropsch synthesis[1, 2, 7, 8], into light olefins or gasoline through methanol as an intermediate[1], or into DME in a single stage[2]. The other alternative is the direct conversion of methane into heavier hydrocarbons by means of oxidative or non-oxidative routes[1, 2, 7, 8]. The use of oxygen for the direct conversion of methane is beneficial as it will increase the reaction rate by shifting the thermodynamic equilibrium. However, kinetically it will limit the yields to the desired primary products that are much more reactive than methane under the experimental conditions used, and will be further converted into combustion products. This has prevented the commercial application of the oxidative methane conversion processes so far[1, 8]. The second direct route for methane conversion is its aromatization under non-oxidative conditions (MDA)[9-11]. Despite the thermodynamic limitations, this process is highly selective to hydrocarbons. The final product composition will depend on the catalyst and on the experimental conditions, and recently conversion of methane to ethylene and aromatics has been reported with selectivity above 99% and no coke formation on lattice-confined single iron sites in a silica matrix[12]. H_2 is formed as a valuable by-product, and its selective removal from the reaction medium may improve the process by shifting the equilibrium controlled reaction. Moreover, the use of the adequate shape-selective catalyst under optimized process conditions may maximize the selectivity to aromatics[10, 11].

The first description of non-oxidative dehydroaromatization of methane in a down-flow fixed bed reactor and in the presence of a bifunctional catalyst was published in the early 1990's[14]. Since then, Mo containing zeolites are still considered as the best catalysts among those described for MDA. Regarding the possible zeolites, the most adequate are those with structures containing pores of dimensions close to the dynamic diameter of benzene, the desired product9. Thus, ZSM-5[11, 15, 16] and MCM-22[11, 17-21] have been thoroughly studied, although other zeolite structures presenting 10-ring channels , such as IM-5[22, 23] or TNU-9[24], have also been recently described for this process. Regarding the reaction mechanism and the active sites involved, it is widely accepted that methane is first activated on the Mo sites and the reaction intermediates formed will further oligomerize, cyclate and dehydrogenate on the Brønsted acid sites.

Catalyst deactivation is one of the main drawbacks of the MDA process[10, 17]. Deactivation is mainly due the formation and deposition of carbonaceous products, largely favored at the high reaction temperatures required for methane activation[25-27]. Moreover, coke formation, mainly on the Brønsted acid sites (BAS) located at the external surface, is widely accepted as the main contributor to catalyst deactivation[28], although some authors also relate the loss of activity to partial sublimation of Mo-oxide phases[29, 30] or transformation of the active phase[31]. In two recent papers, Zhang et al[32, 33] have suggested that although polycondensation of aromatics will be the main contribution to coking of the external surface in the first stages of the reaction, oligomerization and/or cracking of ethene, the main product at longer TOS when benzene formation is significantly reduced, will be responsible for the increasing coke formation rate.

Several approaches can be found in the literature to extend the MDA catalyst life. On the one hand different reactors have been proposed, such as fluidized bed reactors with two differentiated zones in the bed for oxidizing and reducing the catalyst[34] or for combining reaction tests with regeneration steps[35], riser reactors combined with a regeneration zone[36-40], where the catalyst is moved from the reaction zone to the regeneration unit, or pressure swing reactors. On the other hand, it has been described that catalyst stability can be enhanced by adding low amounts of CO/CO_2 to the methane feed due to efficient inhibition of coking[41]. Regarding effective catalyst regeneration processes, the addition of small amounts of NO has been shown to promote coke removal, allowing lower regeneration

temperatures[42]. The use of hydrogen regeneration cycles has also been described[37, 38]. A recent paper evidences the reversible character of isolated Mo oxide nanostructures conversion into carbide Mo nanoparticles, and full recovery of initial Mo species and catalytic activity by regeneration with gas-phase oxygen under proper conditions [43].

In this paper, we present an effective protocol to extend the catalyst life by combination of short reaction-regeneration steps. We present the approaches followed to design this cyclic procedure and we show that restoring the molybdenum-oxo-carbides after each regeneration step and before reaching the reaction conditions is key in order to maximize benzene yield.

2. Experimental

2.1. Catalyst preparation

The parent zeolites used in this work were synthesized following the procedures described in the literature, except for zeolite ZSM-5, which is a commercial sample supplied by TRICAT Inc. in its ammonic form (TZP-302A, Si/Al = 10).

MCM-22 zeolite[44] with Si/Al = 15 was prepared and converted to its acid form as described by Corma et al.[45, 46] employing hexamethyleneimine (HM) as organic structure-directing agent (OSDA). The molar composition of the synthesis gel was 0.5 HM : 44.9 H_2O : 0.18 Na : 0.31 OH : 0.033 Al_2O_3 : 1 SiO_2. The crystallization was carried out in a stainless steel Teflon-lined autoclave at 423K, under agitation (60 rpm) and autogenous pressure for 7 days. After this time, the solid was recovered by filtration, washed repeatedly with deionized water, and dried overnight at 373K, followed by calcination in air at 853K for 3 h to remove the occluded organic SDA in the inner pores. The zeolitic material was refluxed in 2.0 M NH_4Cl solution to exchange the Na^+ by NH_4^+ and finally calcined 773K for 3 h. This procedure was repeated twice in order to obtain the sample in its acid form.

TNU-9 zeolite was synthesized under hydrothermal conditions following the procedure reported by Hong et al.[47] 1,4-Dibromobutane (1,4-DBB, 99% Aldrich) and 1-methylpyrrolidine (1-MP, 90.7% Aldrich) are used as OSDAs, and the molar gel composition was fixed to 4.5 (1,4-DBB) : 13.5 (1-MP) : 11 Na_2O : 0.5 Al_2O_3: 30 SiO_2: 1200 H_2O. The gel was introduced in stainless steel Teflon-lined autoclaves and heated at 433K, under agitation (60 rpm) and autogenous pressure for 8 days. After this period, the solid products were recovered by filtration, washed

repeatedly with deionized water, and dried overnight at 373K, followed by calcination in air at 823K for 3 h to remove the OSDAs. The calcined sample was refluxed in 1.0 M NH_4Cl solution, at 353K for 6h, washed thoroughly with deionized water until chloride free, and then calcined at 773K for 3 h in order to obtain the acid zeolite.

IM-5 zeolite was synthesized following the procedure described by Benazzi et al.[48] employing 1,5-dimethyl-pyridinium bromide (DPB) as OSDA, and the synthesis gel has the following molar composition: 60 SiO_2 : 1.5 Al_2O_3 : 17 Na_2O : 6 NaBr : 10 DPB : 2400 H_2O. The gel was crystallized in a stainless steel Teflon-lined autoclave at 433K under agitation (60 rpm) and autogenous pressure for 10 days. After this period, the solid products were recovered by filtration, washed repeatedly with deionized water, and dried overnight at 373K, followed by calcination in air at 853K for 3 h to remove the OSDA. The acid zeolite was obtained by ion exchange in a 2.0 M NH_4Cl solution at 353K for 2 hours, washed with deionized water until chloride free and followed by calcination at 773K for 3 h.

The molybdenum containing catalysts with a metal loading of 6 wt% were prepared by incipient wetness impregnation of the zeolite with an aqueous solution of ammonium heptamolybdate tetrahydrate (AHM, Merck). After the impregnation, the catalyst was dried at 373K overnight and calcinated in air at 773K for 3 h.

2.2. Characterization techniques

Fresh samples were characterized by X-ray power diffraction (XRD) recorded in a Philips X'Pert diffractometer equipped with a graphite monochromator, operating at 40 kV and 45 mA, and using nickel-filtered CuKα radiation (λ = 0.1542 nm).

The chemical composition of the catalysts was analysed in a 715-ES ICP-Optical Emission spectrometer, after dissolution of the solids in a HNO_3/HF solution.

Textural properties were determined from the nitrogen adsorption isotherm, measured at 77K on a Micrometrics ASAP 2010 volumetric adsorption analyser. Surface area and micropore volume values were obtained by applying the BET equation[49] and from de t-plot graph[50] respectively.

The acidic properties were studied by FT-IR spectroscopy using pyridine as the probe molecule. Pyridine adsorption–desorption experiments were carried out on self-supported

wafers (10 mg/cm) of samples activated at 673K and 10^{-2} Pa for 2 h. After wafer activation, the base spectrum was recorded, and pyridine vapour (6.5×10^{2} Pa) was admitted into the vacuum IR cell and adsorbed onto the zeolite. Desorption was performed under vacuum over three consecutive 1 h periods of heating at 523, 623, and 673K, each followed by an IR measurement at room temperature. All the spectra were scaled according to the sample weight. The amount of Brønsted and Lewis acid sites was determined from the intensities of the bands at ca. 1545 and 1450 cm^{-1}, respectively, using the molar extinction coefficients given by Emeis[51].

The morphology and the topology of the Mo/zeolites were examined by scanning electron microscopy (SEM) with a JEOL 6300 microscope operating at 20 kW, and working with two different detectors, a secondary electron (SE) detector to examine the morphology of the zeolite crystals, and a backscatter electron (BSE) detector in order to study the dispersion of the molybdenum species on the surface of the zeolites.

Hydrogen temperature-programmed reduction (H_2-TPR) was performed in a Micromeritics Autochem 2910. The sample (100 mg) was pretreated in argon flow at room temperature for 30 min, then the gas was switched to the reduction mixture (10 wt.% H_2 in Ar) with a flow rate of 50 ml/min, and temperature was increased to 1373K at a heating rate of 10K/min. The H_2 consumption was followed by a thermal conductivity detector (TCD). No sublimation of molybdenum species was observed during the H_2-TPR experiments, in agreement with previous descriptions[52].

The temperature programmed oxidation analysis (TPO) was used to determine the required temperature to start the coke removal. First the coked catalyst (ca. 100 mg) was pre-treated in helium flow (30 ml/min) for 30 min at 373K to remove absorbed water. After cooling to room temperature a synthetic air flow (100 ml/min) was stabilized, and the temperature was increased with a heating rate of 10K/min to 813K and maintained for two hours, finally the temperature was raised to 1073K at the same heating rate. The TPO experiment was carried out in a Micrometrics Autochem 2920 analyzer comprising a TCD and coupled to a OmniStar quadrupole mass spectrometer (Balzers Instruments) to monitor the evolution of the species CO (m/e = 28), H_2O (m/e = 18) and CO_2 (m/e = 44).

Thermogravimetric and derivative thermogravimetric (TG-DTG) analysis were performed in a Netzch SAT409 EP coupled to a thermobalance, charging 1-5 mg of sample and increasing

temperature form ambient to 1073K under air flow (35 ml/min) with a heating rate of 10K/min.

A EUROEA elemental analyzer (Eurovector) was used in order to determine the carbon content of the used catalysts, before and after being regenerated.

2.3. Methane dehydroaromatization experiments

Dehydroaromatization of methane was performed in a continuous down-flow fixed-bed reactor, at atmospheric pressure, 973K and a contact time of 16 g cat·h/mol CH_4, adjusted to a catalyst weight of 0.5 g. The zeolite based catalyst was diluted with silicon carbide (SiC) to a constant bed volume of 2.8 cm^3. The reactor outlet stream is analysed online by means of a gas chromatograph (Bruker GC-450) provided with two independent channels and three detectors. The permanent gases (N_2 as internal standard, H_2, CO, CO_2) and CH_4 are analysed in a first channel equipped with a TCD and three columns, a Hayesep N (0.5 m length), Hayesep Q (1.5 m) and a 13X molecular sieve (1.2 m length). In a second channel the C1-C4 hydrocarbons were first separated from the aromatics in a CP-Wax capillary column (1.0 m length and 0.32 mm inner diameter). The gases were separated in a CP-Porabond Q (25 m length and 0.32 mm inner diameter) and detected in a FID, whereas the aromatics were separated in a second CP-Wax (5.0 m length and 0.32 mm inner diameter) connected to a second FID. This specific configuration allows on-line determination of the reactor outlet composition during the catalytic reaction and also along the catalyst regeneration step. Yields and selectivities to the different products are given on a carbon basis. The amount of carbonaceous deposits on the catalyst was calculated as the difference between the carbon at the inlet and at the outlet of the reactor as determined from the on-line GC analyses, by co-feeding N_2 (20 mol.%) as internal standard. The specific cyclic reaction-regeneration procedures employed (flows, heating rates and time periods) will be detailed in the corresponding sections of the present paper.

In this reaction system, we also carried out an experiment in order to determine the methane consumption during the activation ramp. Thus, 0.5 g of Mo/ZSM-5 catalyst were charged into the reactor and diluted with CSi to a total bed volume of 2.8 cm^3. The methane:N_2 mixture (CH_4:N_2 = 80:20 in vol.%) was fed to the system with a flow of 15 ml/min, and the reactor was

heated from room temperature to 973K at a rate of 1K/min. The methane consumption was followed by online gas chromatography of the reactor outlet stream.

3. Results and discussions

This section has been divided in three different parts. Initially a reference Mo/ZSM-5 is described and tested under conventional MDA reaction conditions. In a second part, a regenerability study is presented for this Mo/ZSM-5 catalyst. Thus, regeneration of the completely deactivated catalyst has been attempted first by in-situ calcination with air in order to determine the stability of the catalyst towards several cycles of this non-optimized reaction-regeneration protocol. Minimum time and temperatures required for complete coke removal by combustion in air and for carburation of MoO_3 to form the active sites have been determined by means of different characterization techniques, and this information has been used to design and optimize a cyclic reaction-regeneration protocol that effectively regenerates the catalyst and increases the productivity of the process by keeping high selectivity to benzene. Finally, this new reaction-regeneration procedure is applied to other medium pore zeolites which have been shown to be active and selective for the MDA reaction in a third section.

3.1. MDA on a reference Mo/ZSM-5 under conventional reaction conditions

Catalyst preparation and characterization

A commercial ZSM-5 zeolite impregnated with 6 wt.% Mo has been studied in the first place and used as a reference catalyst for this work. The parent zeolite has a Si/Al ratio of 10 and an average crystal size around 900 nm as previously reported[53] . Its textural properties are given in Table 1, together with those corresponding to the Mo-loaded sample. Molybdenum incorporation produces a decrease of the BET surface and the micropore surface and volume in comparison with the parent sample. This fact is mainly attributed to partial blocking of the micropores by the supported MoO_3 particles and to the migration of the Mo species into the channels during the calcination by decomposition of the ammonium heptamolybdate (AHM) used as molybdenum precursor[54-58]. The driving force of this molybdenum migration inside of

the microporous structure has been related to the presence of Brønsted acid sites, since the MoO_3 reacts stoichiometrically 1:1 with H^+ atoms at exchange sites to form $(MoO_2(OH))^+$ species[54, 59], which are the precursors to the active MoC sites required for catalytic C-H bond activation[43].

Structural integrity of the zeolite is preserved after metal impregnation and diffraction peaks related to the presence of MoO_3 are not detected, indicating a high dispersion degree of the Mo species on the zeolite surface[55, 57] according to the XRD patterns (see Figure S1-A in Supplementary material) and the SEM images obtained with a backscatter electron (BSE) detector (Figure S2-A1,A2).

The Brønsted and Lewis acid site density and strength distribution of the ZSM-5 sample, without and with Mo, is shown in Table 2. It can be seen that impregnation with Mo results an important loss of Brønsted acid sites. This decrease can be related to pore blocking by MoO_3 crystals and the consequent inability of pyridine to access and interact with the acid proton, but also to the interaction of these protons with isolated Mo species. It is important to remark that, despite the decrease in the number of Brønsted acid sites, the proportion of stronger sites, able to retain pyridine at 673K, is in the same range before and after Mo incorporation.

Catalytic behavior under conventional MDA reaction conditions

Methane conversion does not only results in the formation of C2+ hydrocarbons, but it also includes the production of carbonaceous species on the catalyst surface, which are MoC_xO_y species formed during the first stage of catalyst activation, and the formation of coke during the second stage of the reaction, when methane activation and aromatization take place. The amount of methane contributing to the formation of these species on the catalyst can be estimated by means of the carbon balance as the difference of the total methane conversion and the total yield to hydrocarbons determined at the reactor outlet. At this point it is important to remark that, unless otherwise specified, in this work the catalyst activation is carried out by increasing temperature in the presence of the methane containing feedstock (CH_4:N_2 = 80:20 in vol.%), so it will be at least partially carburated when the reaction temperature is reached. According to TG-DTA measurements and elemental analysis (EA), the Mo/ZSM-5 catalyst activated with the feed mixture contains 0.8 and 1.1 wt% of carbonaceous

species, respectively, when it reaches the reaction temperature after being activated in the methane feed. During this activation step no hydrocarbons are detected at the reactor outlet stream by on-line gas chromatography at T<973K, so we can assume that the methane consumed has formed the active Mo-oxo-carbide species, and that when starting the MDA reaction, the feedstock finds the catalyst in a carburated form.

In this section we present the catalytic results obtained with the reference Mo/ZSM-5 catalyst under conventional dehydroaromatization conditions (T = 973K, m/F = 16 gcat·h/mol CH_4). Methane conversion, total hydrocarbon yield and the estimated yield to coke versus time on stream (TOS) are shown in Figure 1. The initial methane conversion obtained, around 13%, is close to the equilibrium conversion determined by means of Aspen Hysys® v.8.0 for a temperature of 973K using the Gibbs free energy minimization approach, and in good agreement with the values given in the literature[10, 60]. The catalyst suffers a severe deactivation with TOS due to the rapid buildup of carbonaceous deposits on the catalysts as previously described[52, 61, 62], and conversion after 5 hours on stream is already below 6.0%. **¡Error! No se encuentra el origen de la referencia.**B shows the variation of selectivity within the reactor outlet stream to the two main hydrocarbon groups obtained: aliphatics (C_2 and C_3, mainly ethylene) and aromatics (benzene, naphthalene and others in lower proportion such as toluene), which are clearly affected by the catalyst deactivation degree. **¡Error! No se encuentra el origen de la referencia.**C shows the evolution of selectivity to the main HC products versus time on stream (TOS). Thus, although aromatics (mainly benzene, but also naphthalene) are the main products during the first two hours, their high selectivity decreases after this initial period, whereas selectivity to aliphatics (mainly ethylene) increases reaching values above 60% after 18 hours TOS. Within the aromatics fraction, benzene is the most desired product because of its multiple applications whereas naphthalene is considered an unwanted byproduct[63]. It is important to note that the aromatics selectivity loss at short TOS is due to a decrease in naphthalene selectivity, while benzene selectivity is increased or remained constant during the first hours TOS. This reduction in the selectivity to the bulkier naphthalene has been ascribed to deactivation of the external Brønsted acid sites, and to the reduction of the effective zeolite pore diameters due to coking[64].

3.2. Regenerability of Mo/ZSM-5 catalyst for MDA

Reference reaction/regeneration cyclic procedure

Calcination in air at temperatures generally above 773K is a well-known regeneration procedure when the catalyst is deactivated by the formation of coke[65, 66]. Thus, in a first attempt, a deactivated MDA catalyst, used for 6 hours TOS under the same conditions as those presented in Figure 1, has been regenerated by "in-situ" calcination in an air flow of 100 ml/min, at 813K for six hours and then cooled down to room temperature. Complete coke removal by means of this procedure was confirmed by thermogravimetric and elemental analysis. Before performing a second reaction test, the catalyst was activated under a 15 ml/min flow of the feed mixture as detailed in the experimental section, purged for 30 min under N_2 flow once the reaction temperature of 973K was reached, and the catalytic test was repeated. The overall methane conversion, the total yield to hydrocarbon products (HC) and the estimated coke yield versus TOS for these two reactions are shown **¡Error! No se encuentra el origen de la referencia.**A-C. The plots show the results obtained for the consecutive reaction cycles as a function of the actual time on stream (TOS). The time corresponding to the catalyst cooling, and to the regeneration and re-activation steps has been left out of the plot for simplicity. A continuous line indicates the evolution of conversion during the consecutive reaction cycles, and from one cycle to the next. It can be seen that the total yield to HC products obtained in the 2nd reaction is higher than the one obtained with the fresh catalyst. Encouraged by the good results obtained we carried out five additional regeneration-reaction cycles and results are also presented in Figure 2. Although methane conversion decreases and the differences from one test to the next increase with the number of cycles, the overall yield to hydrocarbons increases for the first three reaction tests.

The evolution of the products' selectivity vs. TOS along the different cycles of reaction plus regeneration is given in **¡Error! No se encuentra el origen de la referencia.**A-B, where the hydrocarbon products have been grouped into aliphatics and aromatics, respectively. The selectivity to both groups is maintained for the first three reaction-regeneration cycles, but after the third cycle, and despite the similar initial values, the selectivity to aliphatics is increased while the selectivity to aromatics is decreased with TOS in a similar proportion, being this effect more accused with the number of cycles. **¡Error! No se encuentra el origen de la referencia.**C and -D show the selectivity to benzene and naphthalene versus TOS respectively. There it can be seen that the loss of aromatics selectivity observed in **¡Error! No**

se encuentra el origen de la referencia.B is mainly due to a decrease of the selectivity to naphthalene, since the benzene selectivity is slightly increased or remains almost constant. Moreover, benzene selectivity is improved not only for all the cycles as compared to the first one during the first two hours TOS -reaction stage known as the induction period[21] - but also along the whole reaction time for the first two consecutive cycles, reaching values of 70wt% on a carbon basis. At longer TOS (≥ 2h) the selectivity to benzene decreases, and the selectivity loss is greater as the number of cycles increases.

Optimization of the reaction/regeneration protocol

What we can learn from the results presented in the former section is that although the Mo/ZSM-5 catalyst suffers an important deactivation since the very early stages of the dehydroaromatization reaction, a high selectivity to the desired benzene is maintained during the first two hours on stream, giving a maximum yield to benzene. Thus, an interesting approach would be to regenerate the catalyst after short times on stream, limited to the induction period (TOS < 2h) described previously. In this way benzene yield may be maximized, and build-up of large carbonaceous deposits will be minimized, facilitating coke removal by means of shorter regeneration times.

As pointed out at the beginning of this section, several tests have been performed with the aim of establishing a suitable reaction-regeneration protocol. First, a temperature-programmed oxidation (TPO) was carried out on a deactivated Mo/ZSM-5 catalyst to estimate the minimum time and temperature required to remove the formed coke. The conditions for complete coke removal will depend on the amount and type of coke, and this, in turn will depend on catalyst composition and on MDA experimental parameters[67-69]. Here, we have limited our study to a single set of reaction conditions, and only TOS will be varied and will have an effect on the coking. Thus, the deactivated catalyst studied here was recovered after being used for 18 h TOS under our MDA reaction conditions, the most severe coking conditions employed in our reaction setup. The TPO test reproduced our conventional regeneration conditions (see the experimental section for more details). By monitoring CO and CO_2 (species m/e = 28 and 44, respectively) in the outlet stream vs. temperature it was determined that coke removal started at 723K, and that after twenty minutes all the carbonaceous deposits were burned off (see **¡Error! No se encuentra el origen de la**

referencia.A). The TPO results were confirmed by performing an *in-situ* regeneration in the fixed bed reactor after a conventional 6 hours run MDA reaction, and determining the composition of the reactor outlet stream by on-line gas chromatography. In good agreement with the TPO results, it was seen that coke was completely removed by treating the deactivated catalyst for no more than twenty minutes at 813K under air flow.

On the other hand, a temperature-programmed reduction in the presence of the methane containing feed (CH_4-TPR, methane mass flow of 8.1 mg/min reproducing catalyst activation conditions, see the experimental section for more details) was performed on the fresh Mo/ZSM-5 catalyst to estimate the temperature at which methane starts to be consumed. This would correspond to the minimum reduction temperature at which MoO_3 would start to be converted into the active molybdenum carbide species. Methane consumption has been represented as a function of temperature in **¡Error! No se encuentra el origen de la referencia.**B, where it is shown to begin at temperatures around 813K. Moreover, no hydrocarbon production was observed during this activation step, so it is assumed that all the methane consumed is contributing to the formation of the active carbides[43].

In the former section, the catalyst was cooled down to room temperature after each regeneration step, and therefore, activation of the catalyst in the methane containing feed flow was started at room temperature. However, the process would gain in efficiency if the catalyst could be activated starting from the regeneration temperature (813K), instead of cooling it down to room temperature and heating it up again. Therefore, in order to rule out any possible effect related to the treatment of the catalyst in the methane flow from room temperature to the regeneration temperature we carried out an additional experiment. Here, the temperature of the catalyst was raised up to 813K under N_2 flow, and then the nitrogen was switched to the CH_4:N_2 mixture until reaching the reaction temperature. No significant differences were observed when comparing activity results or selectivity to aliphatics, aromatics, benzene or naphthalene on both tests (see Figure S3 in Supplementary material).

In view of these results, our proposed protocol of short reaction plus short regeneration steps is the following: the first step is the initial catalyst carburation, heating from room temperature to 973K with a heating rate of 10K/min in a gas mixture flow of methane (80 vol.%) and nitrogen (20 vol.%) in order to start the formation of the molybdenum carbides. When the reaction temperature is achieved, the catalyst is purged with N_2 for 15 min, and

then the CH_4:N_2 flow is fed using the same composition employed before for carrying out the MDA reaction (80:20 vol.%). After 1.5 h of reaction, the catalyst is cooled in nitrogen flow down to the regeneration temperature. Coke removal is carried out at 813K for 30 min under oxygen (21 or 10 vol.% of O_2 in N_2) with a total gas flow of 100 ml/min. Thermogravimetric (TG) and elemental analysis (EA) were performed at this point to verify that the carbonaceous deposits of the catalyst were completely removed. After the regeneration step the catalyst is purged with nitrogen for 15 min at 813K, followed by re-carburation of the catalyst in the CH_4:N_2 mixture for 10 min at 813K. Finally, the sample is heated to 973K in the feed mixture with a heating rate of 10K/min to start a new cycle.

In order to determine if the catalyst re-carburation step makes a difference, we have applied the same procedure but leaving out the re-carburation step and heating the catalyst from the regeneration temperature to the reaction temperature under nitrogen flow on our reference Mo/ZSM-5 catalyst. A diagram showing a single cycle of our protocol, with and without the re-carburation step, is shown in Figure 5.

The results obtained using the 1.5h reaction-0.5h regeneration protocol regenerating in 10 and 21 vol.% of O_2, activating in methane, and the same procedure regenerating in 10 vol.% O_2, but in this case activating the catalyst in N_2 are shown in Figures 6 and 7. The single conventional 18 h TOS experiment is included for comparison purposes.

Figure 6A shows the methane conversion obtained for the consecutive reaction cycles as a function of the actual time on stream (TOS). The time corresponding to the catalyst cooling, and to the regeneration and re-activation steps has been left out of the plot for simplicity. A dotted line indicates the evolution of conversion during the consecutive reaction cycles, and from one cycle to the next. Thus, an initial methane conversion close to 13.0% is obtained, and activity decreases sharply with TOS down to ≈ 8.0%, in line with the results obtained for the conventional MDA run. After the regeneration and re-activation conversion is recovered and even increased as compared to that of the fresh catalyst, and deactivation rate is similar to that of the first cycle. As the number of cycles increases, the initial methane conversion gets lower, and deactivation rate increases slightly. Regarding the product yields, Figure 6B shows the evolution of the total HC yield along the different cycles, considering only the time the catalyst is on stream for the MDA reaction. Despite the decrease of the initial HC yield as the number of cycles increases, the values obtained are far above those corresponding to the

conventional MDA run. It can also be seen that the estimated yield to coke at the beginning of each of the cycles is mainly constant (Figure 6C).

Although the regeneration procedure proposed recovers most of the initial catalyst activity after each cycle, independently of the O_2 content in the regeneration stream, and of the composition of the activation stream –pure N_2 or CH_4:N_2 mixture-, there are some differences among the experiments compared. When the sample is activated in the methane feed flow the conversion levels achieved are higher than when it is activated in an inert flow. The total yield to HC is also higher when the catalyst is carbureted during the activation, whereas the estimated coke yield is similar in both cases, indicating larger coke selectivity when the catalyst has to be re-carburated after reaching the reaction temperature. Thus, activating in methane results in a more efficient conversion of the feed into the desired HC during the reaction step. Regarding the effect of the oxygen concentration during regeneration, the initial conversion levels achieved when decreasing O_2 partial pressure are lower as compared to the higher O_2 concentration, but this is mainly due to a lower coke yield when O_2 proportion is reduced during the intermediate regeneration steps, and the production of hydrocarbons is comparable in both cases. Thus, a lower O_2 concentration in the regeneration stream seems to preserve in a larger extend the distribution of the active molybdenum species.

The selectivity to aliphatics (A) and aromatics (B) is shown in Figure 7. It can be seen that although the former increases with TOS along each of the cycles, the proportion of aliphatics is kept reasonably low along the total process, whereas the selectivity to aromatics is maintained in the range of 85-95 wt%. Again, activation of the catalyst in the feed stream results in an improved catalytic behavior, with lower selectivity to aliphatics and higher production of aromatics. Regarding the aromatic's distribution, the catalyst activated in nitrogen is slightly more selective to benzene and less to naphthalene. This could be due to a lower Brønsted acid site density, as will be discussed later. The oxygen concentration during regeneration has no significant effect on the product distribution.

The results presented in Figure 6 and Figure 7 show that is possible to extend the life of the catalyst with the described reaction-regeneration cyclic procedure, as the overall conversion of methane, the total yield to hydrocarbon products' (HC) and, most important, the selectivity to aromatics -especially to benzene-are maintained for a longer time. At this point we have

estimated a benzene productivity (g benzene/kg cat·h) for different periods on stream, performed in a single run and in 12 consecutive cycles of our 1.5 h reaction-0.5 h regeneration protocol. The productivities obtained are given in Table 3. It can be seen that productivities obtained with the two procedures are not so different when a short 6h period is considered. However, due to the drastic deactivation of the catalyst at long reaction times, when the period of TOS considered is increased to 12 and 18 h, the productivity obtained with a single run decreases significantly, whereas almost constant productivity is obtained when applying the new cyclic protocol presented in this work. For the longest period considered, of 18 h TOS, benzene productivity obtained with the optimized cyclic reaction-regeneration procedure triplicates the one of the conventional 18 h MDA experiment (97 vs 33 g benzene/kg cat·h, respectively).

Regarding the need for an intermediate re-carburation, we have shown that when N_2 is used instead of methane during the catalyst activation step and the catalyst is not re-carburated during the activation, the total methane conversion is lower, the deactivation effect is more accused, and the selectivity to aromatics is lower (see Figure 6 and 7). This behavior can be attributed to the fact that during the regeneration not only coke is removed, but also the oxo-carbides responsible for methane activation are lost. Thus, after regeneration the active carbide species will have to be formed again. When the catalyst is activated in N_2, the carbides will start to be formed at 973K, once the catalyst has reached the reaction temperature and the methane feed is introduced in the system. Thus, at some point the dehydroaromatization of methane will be competing with the formation of the active species on the catalysts. On the other hand, if the catalyst is activated in the presence of a methane containing flow, the active species start to be formed at a lower temperature, and when the catalyst reaches the reaction temperature most of the molybdenum species will be already reduced and in its active oxocarbide form.

Characterization of spent catalysts

First of all, it is important to remark that the used catalysts after the different reaction-regeneration procedures present the same Mo content as the corresponding fresh catalyst, indicating that the molybdenum species have not sublimated during our experimental conditions (see the chemical composition in Table 1). On the other hand, complete coke

removal on the different regenerated catalysts was confirmed before performing the rest of characterization. Regarding the textural and acidic properties, all the catalysts, after being used under the different reaction-regeneration procedures, present a decrease in BET surface, micropore surface and volume, and a lower total number of Brønsted acid sites in comparison with the fresh catalyst (see Table 2). However, the loss of microporosity is lower for the short reaction-regeneration protocol when the catalyst is activated in methane instead of N_2, and its Brønsted acidity is higher. When compared to the long reaction-regeneration cycles, the new protocol proposed preserves the zeolite structure in a larger extend (higher BET and micropore surface area) but Brønsted acidity is higher for the former (Table 2), and also the proportion of stronger Brønsted acid sites, able to retain pyridine at 673K. A possible explanation could be a better dispersion of the Mo-species (lower agglomeration degree), and therefore a higher interaction with the Brønsted sites (leaving less H^+ available) when the short reaction-regeneration procedure is employed. In fact, this is in good agreement with recent studies on the effect of regeneration time with O_2, that show how longer regeneration times do restore the Mo oxide nanostructures, but forces them to migrate from Al framework sites to Si anchoring sites on the external surface of the zeolite[43]. This would restore the Brønsted acid site corresponding to the framework Al. Moreover, the formation of less coke and of a coke less refractory in nature could also result in lower local temperature spots due to the exothermic combustion reaction, and thus, to a better structure preservation when using the optimized cyclic reaction-regeneration procedure.

Regarding the effect of O_2 concentration during the regeneration step, it has a clear effect on the physico-chemical and acidic properties of the spent catalyst (see Tables 1 and 2), and a decrease in O_2 content from 21 to 10 vol.% results in a final catalyst with higher BET, higher micropore surface and higher total Brønsted acidity, probably due to the less severe coke combustion conditions. Moreover, the proportion of strong Brønsted acid site, given by the ratio B673/B523 in Table 2, increases when lowering the O_2 concentration in the regeneration stream to values close to those of the fresh catalyst.

The main differences among the catalysts used under different reaction-regeneration conditions have been found to be related to the nature and the reducibility of their molybdenum species, as determined by H_2-TPR experiments. According to the literature[61, 62, 70] four regions are detected based on the Mo reduction temperature: (I) 473-650K related to

the partial reduction of amorphous polymeric molybdate species, (II) 650-875K ascribed to the reduction of MoO_3 to MoO_2, (III) 875-1173K assigned to the reduction of MoO_2 to Mo^0, and finally the region (IV) >1173K related to the reducibility of the $[Mo_2O_3]^{+2}$ species occluded inside of the zeolitic channels, and therefore more difficult to be converted. Figure 8 shows the H_2-TPR profiles corresponding to Mo/ZSM-5 before and after being used on six cycles of 6h reaction plus 6h regeneration and after the 1.5 h reaction-0.5 h regeneration protocol employing 10 vol.% of O_2 in the regeneration step. The fresh Mo/ZSM-5 presents a typical H_2-TPR profile, with peaks in all the regions previously described. However, the used Mo/ZSM-5 after six cycles (6 h reaction + 6 h regeneration) only shows one peak in the region of the conversion of MoO_3 to MoO_2, and the profile has been shifted to higher temperatures indicating that the Mo species are more difficult to be reduced. On the other hand, the H_2-TPR profile of the used catalyst after short reaction-regeneration protocol is more similar to that of the fresh catalyst, indicating a larger preservation of both, the nature and the reducibility of the Mo species present, when using our optimised protocol.

3.3. Application of the optimized reaction/regeneration protocol to other medium pore zeolites

In view of the interesting results obtained in the former section, we decided to apply our optimized 1.5 h reaction-0.5 h regeneration protocol to other medium pore zeolites which have been described for the MDA reaction, such as Mo/MCM-22, Mo/TNU-9 and Mo/IM-5[11, 17-24]. The procedure employed in this section is the one using a 10 vol.% of oxygen in nitrogen during the regeneration step and re-carburating the catalyst after the regeneration, the procedure that was found to be less detrimental regarding the catalysts' properties (highest micropore structure and Brønsted acid site preservation).

Catalyst preparation and characterization

The parent zeolites compared in this section present a Si/Al molar ratio close to 10 and crystal sizes in the submicron range (see SEM images presented in Figure S1). The three samples have been impregnated with molybdenum (6 wt%) by incipient wetness, following the same procedure used for preparation of the Mo/ZSM-5 catalyst studied previously. Their chemical

composition is shown in Table 4, where it can be seen that the Mo/Al ratio is in all cases close to 0.5. This value has been described as optimum to balance the methane activation and the aromatization reactions, giving conversion of the ethylene formed close to-equilibrium levels on the remaining Brønsted acid sites[54].

As in the case of Mo/ZSM-5, the molybdenum incorporation does not affect the crystallinity of the zeolitic structure and the metallic phase is homogeneously dispersed for all of catalysts, since diffraction peaks related to the presence of MoO_3 were not detected (see XRD patterns presented in Figure S2), and SEM images obtained with a backscatter electron (BSE) detector do not show the presence of large spots corresponding to MoO_3 agglomerates (see Figure S1). However, the molybdenum loading results in a decrease of the BET surface, the micropore surface and volume, and the total number of Brønsted acid sites as compared to the parent sample. This fact can be related to the partial blocking of the micropores by the supported MoO_3 particles, and to the migration of Mo species into the zeolite channels during the calcination, as described previously for Mo/ZSM-5 (see Table 4 and Table 5). Unlike the case of Mo/ZSM-5, when Mo was impregnated on IM-5, TNU-9 and MCM-22, not only the total amount of Brønsted acid sites was reduced, but also the proportion of the stronger ones.

Catalytic results applied to Mo/IM-5, Mo/TNU-9 and Mo/MCM-22

The results obtained using the new reaction-regeneration cycles, regenerating in a 10 vol.% oxygen in nitrogen stream, and re-carburating the catalyst before reaction are shown in Figure 9 for catalysts Mo/IM-5, Mo/TNU-9 and Mo/MCM-22, respectively, and compared with Mo/ZSM-5 tested under the same conditions. With the aim of simplifying the figure, only the first point of each cycle is plotted vs. TOS. In this way, activity and selectivity results obtained for the four catalysts can be directly compared. However, the full plots, including the complete cycles as well as the conventional single run for each of the catalysts are given as Figures S4-S6 in the supporting information, where it can be seen that, as in the case of Mo/ZSM-5, the cyclic reaction-regeneration protocol effectively improves the process by increasing the yield to aromatics, especially benzene, and by extending the life of the Mo/zeolite, as compared to a conventional single run of at least 12 h TOS.

Mo/IM-5 shows some deactivation degree, with initial methane conversion being reduced after each cycle, and its behavior is comparable to that of the reference catalyst Mo/ZSM-5

(see Figure 9 and S4). Its yield to HC is fairly constant, and initial benzene selectivity is improved when increasing the number of cycles. Mo/TNU-9 shows a very good performance, with activity being completely recovered after each cycle, with constant initial HC yield, and with a high benzene selectivity that increases after each reaction-regeneration cycle (see Figures 9 and S5).

Finally, the results obtained with Mo/MCM-22, also compared in Figure 9, show a very good recovery of the initial methane conversion after each cycle. This catalyst is known to be more stable towards deactivation[21] than Mo/ZSM-5, and benzene selectivity is maintained around 80% for almost 5 hours TOS during the single run (see Figure S6). Thus, the cyclic reaction-regeneration protocol optimized for Mo/ZSM-5 could be improved for Mo/MCM-22 by increasing the time of the reaction step. This would increase the overall benzene production.

Characterization of spent catalysts

Table 4 compares the physico-chemical and acidic properties of the parent zeolites, the fresh Mo-containing catalysts and the spent samples. It can be seen that Mo/TNU-9 presents the largest micropore volume after Mo loading, not only before, but also after being used in the MDA reaction. This can be due to a better Mo distribution, probably closer to the external surface or in the pore mouths. It is possible that the specific microporous structure, the very small crystallite size of the parent zeolite, and perhaps the Al distribution within the crystals will be responsible for the highly interesting catalytic behaviour of Mo/TNU-9 for methane hydroaromatization by means of this new reaction-regeneration cyclic protocol. The effect of the zeolite structure is, however, out of the scope of the present work, and will be thoroughly covered in a future paper. Regarding the Brønsted acid site density, presented in Table 5, when we compare the values corresponding to the fresh catalysts and to those used for the cyclic reaction-regeneration procedure, the number of acid sites is preserved in a larger extend in the cases on Mo/TNU-9 and Mo/IM-5 than on Mo/MCM-22 or on the reference Mo/ZSM-5. Again, the structure and/or Al distribution can be playing an important role. Regarding the strength distribution of the Brønsted acid sites, in all cases we observe a good preservation of the proportion of the strongest sites among the total Brønsted acid site density (see Table 5), as we also observed for Mo/ZSM-5. So we can conclude that the new

cyclic protocol does not affect the acid strength distribution of the regenerated catalyst as compared to the fresh Mo/zeolite.

4. Conclusions

An effective procedure has been proposed to extend the life of a conventional Mo/ZSM-5 catalyst for methane dehydroaromatization by a short reaction-regeneration cyclic operation. The method, optimized for a Mo/ZSM-5 catalyst, combines 1.5 h reaction periods with 0.5 h regeneration steps in a continuous cyclic mode, which allow maximizing the benzene yield (the most desired product) for longer times in comparison with a conventional single run experiment. After each regeneration stage the catalysts were purged with nitrogen and re-carburated by increasing temperature in the methane containing feed mixture. This step was seen to play an important role in the effectiveness of the cyclic reaction-regeneration procedure. With this optimized cyclic operation protocol, it has been possible to increase the benzene productivity obtained on a Mo/ZSM-5 catalyst during 18 h on stream from 33 g benzene/kg cat·h for a single 18 h run to 97 g benzene/kg cat·h when performing the reaction for 12 cycles of 1.5 h TOS.

The protocol has proved to be efficient not only for Mo/ZSM-5, but also for other promising medium pore zeolites for MDA reaction, such as Mo/MCM-22, Mo/TNU-9 and Mo/IM-5. Among the catalysts compared, Mo/TNU-9 shows an outstanding behavior, with constant initial activity for each new cycle, constant initial HC yield, and a high benzene selectivity (≈ 85% average) that increases not only with TOS, but also after each reaction-regeneration cycle. Moreover, the effectiveness of the procedure could be improved by optimizing the length of the regeneration and/or the reaction steps for the different catalysts.

Acknowledgements

Funding from the European Community's 7th Framework Program through the Collaborative Project Next-GTL (agreement n° 229183) and financial support by the Spanish Government-MINECO through "Severo Ochoa" (SEV 2012-0267), Consolider Ingenio 2010-Multicat, MAT2012-37160 and MAT2012-31657 are acknowledged. The authors thank B. Esparcia for

technical assistance, and the Electron Microscopy Service of the UPV for their help in samples characterization.

References

1. I.H. Lunsford, *Catal. Today*, 2000, **63**, 165-174
2. E.F. Sousa-Aguiar, L.G. Appel, C. Mota, *Catal. Today* 2005, **101**, 3-7
3. A. Caballero, P.J. Pérez, *Chem. Soc. Rev.*, 2013, **42**, 8809-8820
4. J.N. Armor, *J. Energy Chem.*, 2013, **22**, 21-26
5. Q. Wang, X. Chen, A.N. Jha, H. Rogers, *Renew. Sust. Energ. Rev.*, 2014, **30**, 1-28
6. D.A. Wood, C. Nwaoha, B.F. Towler, *J. Nat. Gas Sci. Eng.*,2012, **9**, 196-208
7. A. Martínez, G. Prieto, A. García-Trenco, E. Peris, in *Zeolites and Catalysis: Synthesis, Reactions and Applications*, eds. J. Čejka, A. Corma, S. Zones, Wiley-VCH Verlag GmbH & Co. KGaA, 2010, pp. 649-685
8. M. Gharibi, F.T. Zangeneh, F. Yaripour, S. Sahebdelfar, *Appl. Catal. A*, 2012, **443-444**, 8-26
9. M.T. Portilla, C.H.L. Tempelman, C. Martínez, E. J.M. Hensen, in *Small-Scale Gas to Liquid Fuel Synthesis*, eds. Nick Kanellopoulos, Taylor & Francis Group, 2015, pp. 263-291
10. J.J. Spivey, G. Hutchings, *Chem. Soc. Rev.*, 2014, **43**, 792-803
11. Z.R. Ismagilov, E.V. Matus, L.T. Tsikoza, *Energ. Environ. Sci.*, 2008, **1**, 526-541
12. X. Guo, G. Fang, G. Li, H. Ma, H. Fan, L. Yu, Ch. Ma, X. Wu, D. Deng, M. Wei, D. Tan, R. Si, S. Zhang, J. Li, L. Sun, Z. Tang, X. Pan, X. Bao, *Science*, 2014, **344**, 616-619
13. S. Ma, X. Guo, L. Zhao, S. Scott, X. Bao, *J. Energy Chem.*, 2013, **22**, 1-20
14. L. Wang, L. Tao, M. Xie, G. Xu, J. Huang, Y. Xu, *Catal. Lett.*, 1993, **21**, 35-41
15. Z.R. Ismagilov, E.V. Matus, M.A. Kerzhentsev, L.T. Tsikoza, I.Z. Ismagilov, K.D. Dosumov, A.G. Mustafin, *Petrol. Chem.*, 2011, **51**, 174-186
16. W. Wei, *J. Nat. Gas Chem.*, 2000, **9**, 76-86+88
17. S. Majhi, P. Mohanty, H. Wang, K.K. Pant, *J. Energy Chem.*, 2013, **22**, 543-554
18. J. Bai, S. Liu, S. Xie, L. Xu, L. Lin, *React. Kinet. Catal. Lett.*, 2004, **82**, 279-286
19. Z. Sobalík, Z. Tvarůžková, B. Wichterlová, V. Fíla, Š. Špatenka, *Appl. Catal. A*, 2003, **253**, 271-282
20. D. Ma, Y. Shu, X. Han, X. Liu, Y. Xu, X. Bao, *J. Phys. Chem. B*, 2001, **105**, 1786-1793
21. Y. Shu, D. Ma, L. Xu, Y. Xu, X. Bao, *Catal. Lett.*, 2000, **70**, 67-73
22. H. Liu, J. Hu, Z. Li, S. Wu, L. Liu, J. Guan, Q. Kan, *Kinet. Catal.*, 2013, **54**, 443-450
23. H. Liu, S. Wu, Y. Guo, F. Shang, X. Yu, Y. Ma, C. Xu, J. Guan, Q. Kan, *Fuel*, 2011, **90**, 1515-1521
24. H. Liu, S. Yang, S. Wu, F. Shang, X. Yu, C. Xu, J. Guan, Q. Kan, *Energy*, 2011, **36**, 1582-1589
25. S. Liu, L. Wang, R. Ohnishi, M. Ichikawa, *Kinet. Catal.*, 2000, **41**, 132-144
26. B. Weckhuysen, M. Rosynek, J. Lunsford, *Catal. Lett.*, 1998, **52**, 31-36.
27. D. Ma, D. Wang, L. Su, Y. Shu, Y. Xu, X. Bao, *J. Catal.*, 2002, **208**, 260-269

28. C. Descorme, P. Gelin, C. Lecuyer, A. Primet, *Appl. Catal. B*, 1997, **13**, 185-195
29. D. Ren, X. Wang, G. Li, X. Cheng, H. Long, L. Chen, *J. Nat. Gas Chem.*, 2010, **19**, 646-652
30. M.C. Iliuta, I. Iliuta, B.P.A. Grandjean, F. Larachi, *Ind. Eng. Chem. Res.*, 2003, **42**, 3203-3209
31. M. Nagai, Nishibayashi, S. T. Omi, *Appl. Catal. A*, 2003, **253**, 101-112
32. Y. Song, Y. Xu, Y. Suzuki, H. Nakagome, Z.-G. Zhang, *Appl. Catal. A*, 2014, **482**, 387-396
33. Y. Xu, Y. Suzuki, Z.-G. Zhang, *Appl. Catal. A*, 2013, **452**, 105-116
34. M.P. Gimeno, J. Soler, J. Herguido, M. Menéndez, *Ind. Eng. Chem. Res.*, 2010, **49**, 996-1000
35. B. Cook, D. Mousko, W. Hoelderich, R. Zennaro, *Appl. Catal. A*, 2009, **365**, 34–41
36. R.J. Gulotty, J.E. Peleti, A.R. Prumier, A.E. Schweizer, US Patent 0312029, 2010, to Dow Clobal Technologies Inc.
37. C. Schneider, M. Karches, J.C. Tsou, S. Abrens, D. Stuetzer, US Patent 0165585, 2012, to BASG SE.
38. F. Kiesslich, J.C. Tsou, A. Schulz, US Patent 0060176, 2011, to BASG SE.
39. L.L. Iacino, N. Sangar, E.L. Stavens, US Patent 0276171, 2007, to Exxonmobil Chemical Company
40. L.L. Iacino, E.L. Stavens, N. Sangar, US Patent 0249879, 2007, to Exxonmobil Chemical Company
41. H. Ma, Y. Ogawa, EP Patent 2140939, 2008, to Meidensha Corporation
42. H. Ma, R. Kojima, R. Ohmishi, M. Ichikawa, *Appl. Catal. A*, 2004, **275**, 183-187
43. J. Gao, Y. Zheng, J.-M. Jehng, Y. Tang, I.E. Wachs, S.G. Podkolzin, Science aaa7048Published online 9 April 2015 [DOI:10.1126/science.aaa7048]
44. M.E. Leonowicz, J.A. Lawton, S.L. Lawton, M.K. Rubin, *Science*, 1994, **264**, 1910-1913
45. A. Corma, C. Corell, F. Llopis, A. Martínez, J. Pérez-Pariente, *Appl. Catal. A*, 1994, **115**, 121-134
46. A. Corma, C. Corell, J. Pérez-Pariente, *Zeolites*, 1995, **15**, 2-8.
47. S.B. Hong, H.-K. Min, C.-H. Shin, P.A. Cox, S.J. Warrender, P.A. Wright, *J. Am. Chem. Soc.*, 2007, **129**, 10870-10885
48. E. Benazzi, J.-L. Guth, L. Rouleau, US Patent 6136290, 2000, to Institut Francais de Petrole
49. S. Brunauer, P.H. Emmett, E. Teller, *J. Am. Chem. Soc.*, 1938, **60**, 309-319.
50. W.D. Harkins, G. Jura, *J. Am. Chem. Soc.*, 1944, **66**, 1366-1373
51. C.A. Emeis, *J. Catal.*, 1993, **141**, 347-354
52. A. Martínez, E. Peris, M. Derewinski, A. Burkat-Dulak, *Catal. Today*, 2011, *169*, 75-84
53. A. Corma, C. Martínez, E. Doskocil, *J. Catal.*, 2013, **300**, 183-196

54. R.W. Borry III, Y.H. Kim, A. Huffsmith, J.A. Reimer, E. Iglesia, *J. Phys. Chem. B*, 1999, **103**, 5787-5796
55. L.Y. Chen, L.W. Lin, Z.S. Xu, X.S. Li, T. Zhang, *J. Catal.*,1995, **157**, 190-200
56. Y.-H. Kim, R.W. Borry III, E. Iglesia, *Micropor. Mesopor. Mat.*, 2000, **35–36**, 495-509
57. D. Wang, J.H. Lunsford, M.P. Rosynek, *J. Catal.*, 1997, **169**, 347-358
58. Y. Xu, Y. Shu, S. Liu, J. Huang, X. Guo, *Catal. Lett.*, 1995, **35**, 233-243
59. W. Ding, S. Li, G.D. Meitzner, E. Iglesia, *J. Phys. Chem. B*, 2001, **105**, 506-513
60. P.M. Bijani, M. Sohrabi, S. sahebdelfar, *Chem. Eng. Technol.*, 2012, **35**, 1825-1832
61. Z. Jin, S. Liu, L. Qin, Z. Liu, Y. Wang, Z. Xie, X. Wang, *Appl. Catal. A*, 2013, **453**, 295-301
62. Y. Song, C. Sun, W. Shen, L. Lin, *Appl. Catal. A*, 2007, **317**, 266-274
63. C. Martinez, A. Corma, *Coordin. Chem. Rev.*, 2011, **255**, 1558-1580
64. S. Kikuchi, R. Kojima, H. Ma, J. Bai, M. Ichikawa, *J. Catal.*, 2006, **242**, 349-356
65. Y. Mathieu, A. Corma, M Echard, M. Bories, *Appl. Catal. A*, 2014, **469**, 451-465
66. S. Laforge, D Martin, J.L. Paillaud, M. Guisnet, *J. Catal.*, 2003, **220**, 92-103
67. E.V. Matus, I.Z. Ismagilov, O.B. Sukhova, V.I. Zaikovskii, L.T. Tsikoza, Z.R. Ismagilov, *Ind. Eng. Chem. Res.*, 2007, **46**, 4063-4074
68. Z.R. Ismagilov, L.T. Tsikoza, E.V. Matus, G.S. Litvak, I.Z. Ismagilov and O.B. Sukhova, *Eurasian Chemico-Technological Journal*, 2005, **7** (2), 115-122
69. E.V. Matus, O.B. Sukhova, I.Z. Ismagilov, V.I. Zaikovskii, M.A. Kerzhentsev, Z.R. Ismagilov, K.D. Dosumov, A.G. Mustafin, *Eurasian Chemico-Technological Journal*, 2010, **12** (1), 1-8
70. H. Liu, X Bao, Y. Xu, *J. Catal.*, 2006, **239**, 441-450

Figure caption

Figure 1. (A) Methane conversion (), total yield to hydrocarbon products () and estimated yield to coke () versus TOS; (B) Selectivity to aromatics ()and aliphatics (), and (C) Selectivity to ethylene (), ethane (), benzene (), toluene () and naphthalene () versus TOS

Figure 2. Methane conversion (A), total yield to HC products (B), and estimated yield to coke (C), versus TOS for six consecutive 6 h reaction – 6 h regeneration cycles.

Figure 3. Selectivity to aliphatics (A), aromatics (B), benzene (C) and naphthalene (D) versus TOS for six consecutive 6 h reaction – 6 h regeneration cycles.

Figure 4. Thermal conditions required for removal (A) and formation (B) of carbon species on coked and fresh Mo/ZSM-5, respectively.

Figure 5. Diagram of the short reaction-regeneration cyclic protocol with (A) and without re-carburation step (B).

Figure 6. Methane conversion (A), total yield to HC products (B), and estimated yield to coke (C), for the short reaction-regeneration cyclic protocol, regenerating under 21vol% oxygen () or 10vol% oxygen () in nitrogen, and without the re-carburation step after the regeneration under 10vol% O_2 in nitrogen () compared to a single 18 h TOS MDA reaction ( )

Figure 7. Selectivity to aliphatics (A), aromatics (B), benzene (C) and naphthalene (D) for the short reaction-regeneration cyclic protocol, regenerating under 21vol% oxygen () or 10vol% oxygen () in nitrogen, and without the re-carburation step after the regeneration under 10vol% O_2 in nitrogen () compared to a single 18 h TOS MDA reaction ( )

Figure 8. H_2-TPR profiles corresponding to Mo/ZSM-5 before and after being used on different reaction-regeneration procedures.

Figure 9. Methane conversion (A), total yield to HC (B), estimated yield to coke (C) for the short reaction-regeneration cyclic protocol, regenerating 10vol% oxygen, over Mo/ZSM-5 ( ), Mo/IM-5 ( ), Mo/TNU-9 ( ) and Mo/MCM-22 ( ).

Figure 1.

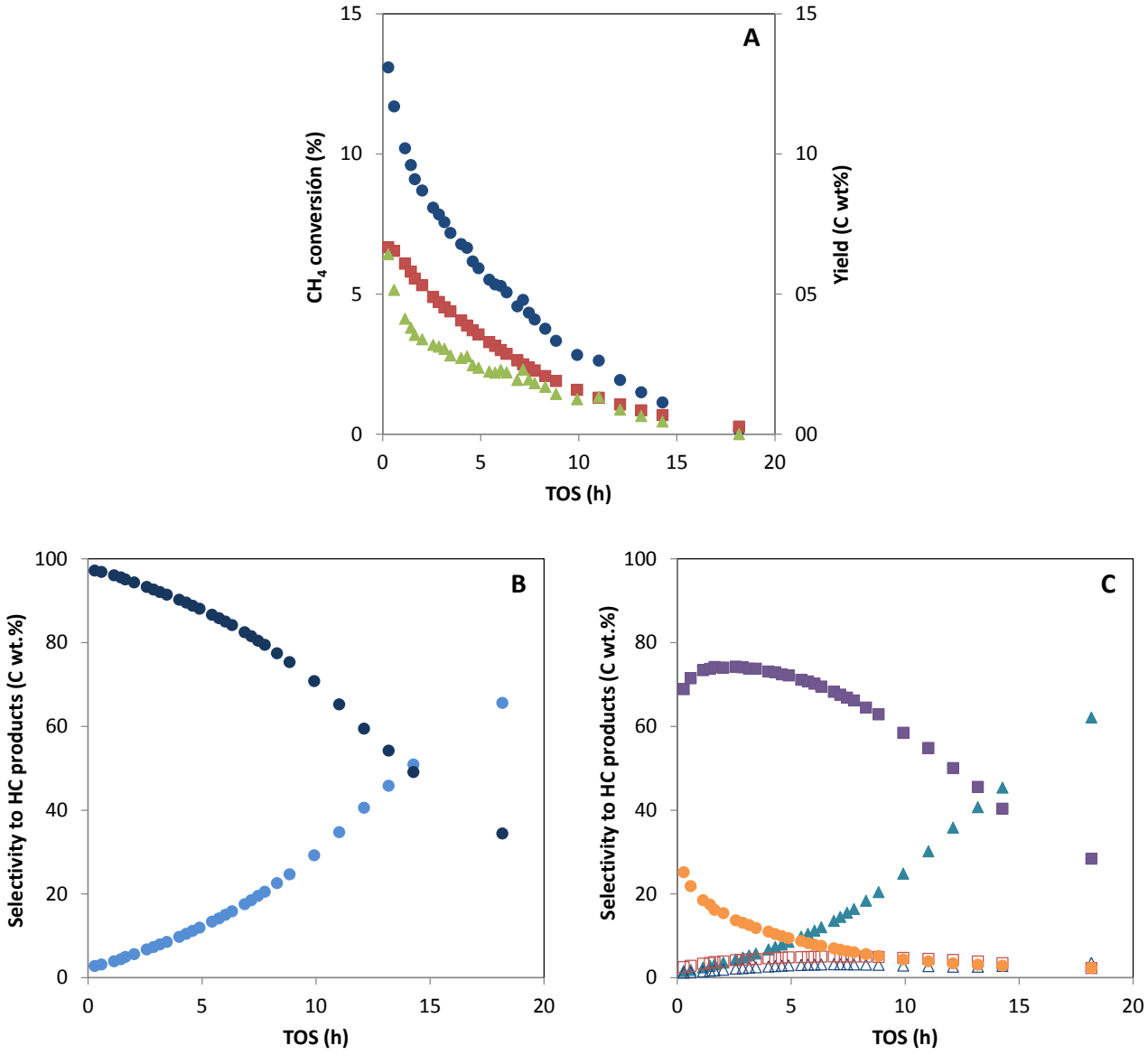
A
B
C
CH4 conversión (%)
Yield (C wt%)
TOS (h)
Selectivity to HC products (C wt.%)
TOS (h)
Selectivity to HC products (C wt.%)
TOS (h)

Figure 2.

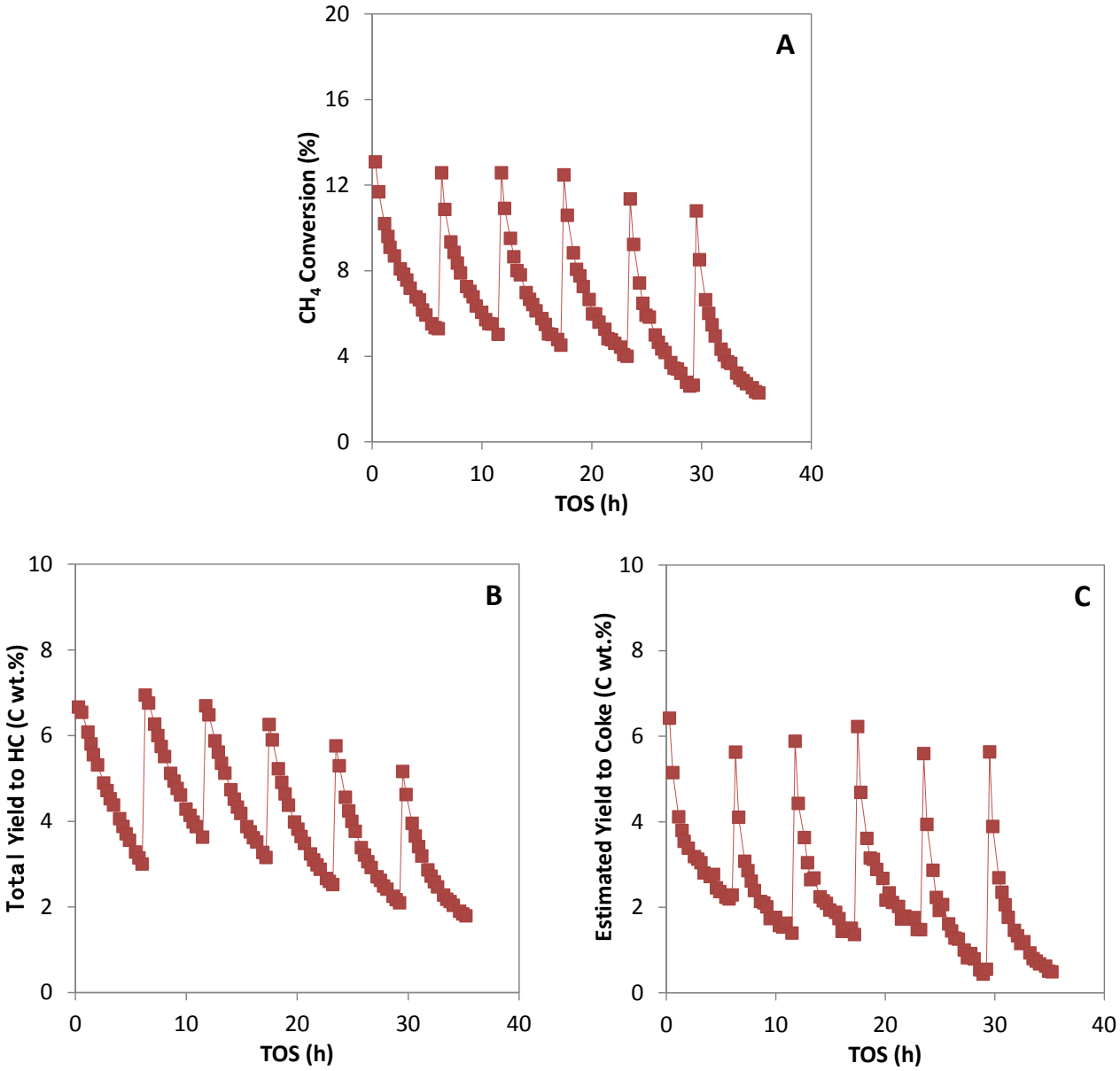
A
CH_4 Conversion (%)
TOS (h)
B
Total Yield to HC (C wt.%)
TOS (h)
C
Estimated Yield to Coke (C wt.%)
TOS (h)

Figure 3.

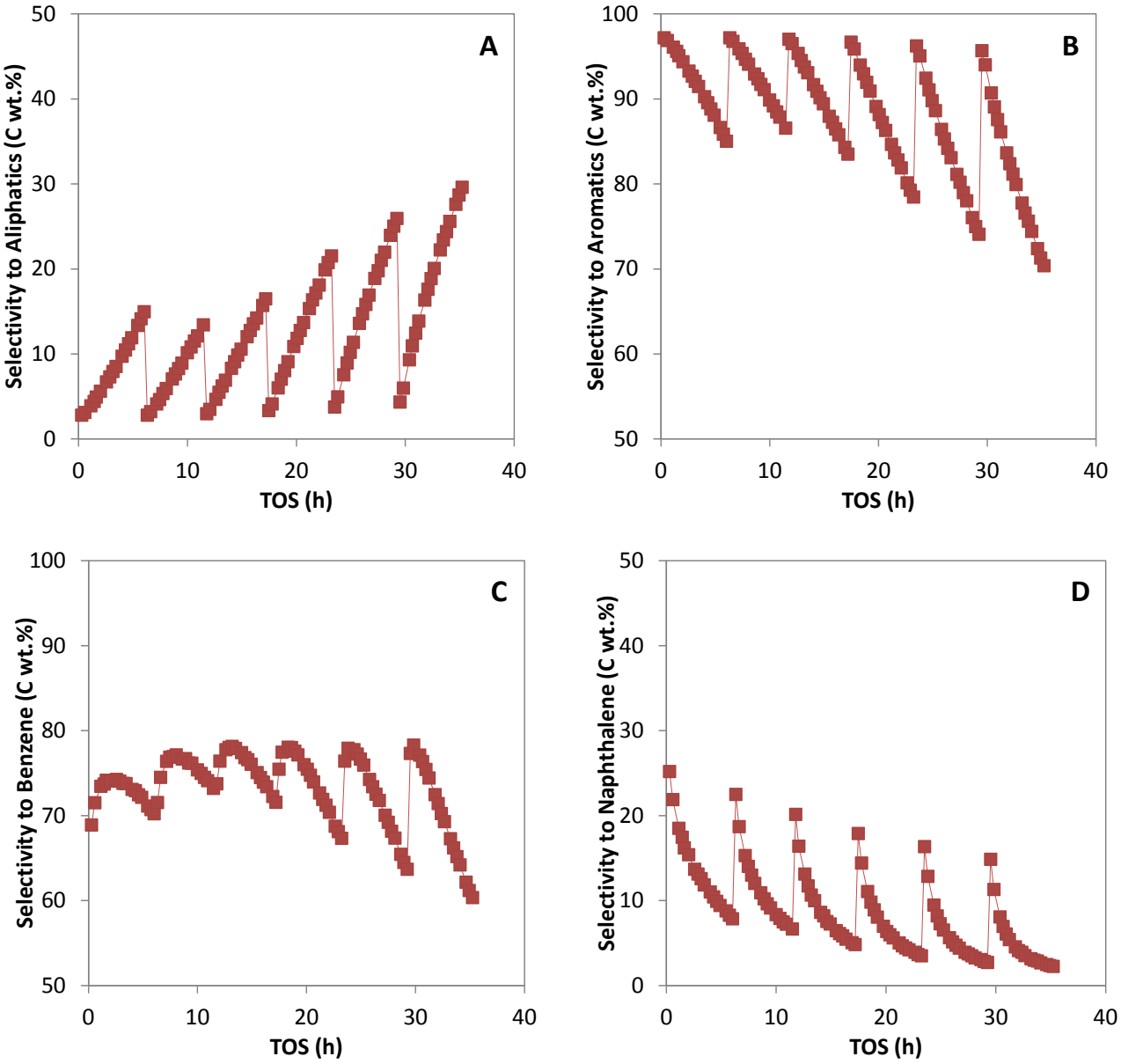
A
Selectivity to Aliphatics (C wt.%)
TOS (h)
B
Selectivity to Aromatics (C wt.%)
TOS (h)
C
Selectivity to Benzene (C wt.%)
TOS (h)
D
Selectivity to Naphthalene (C wt.%)
TOS (h)

Figure 4.

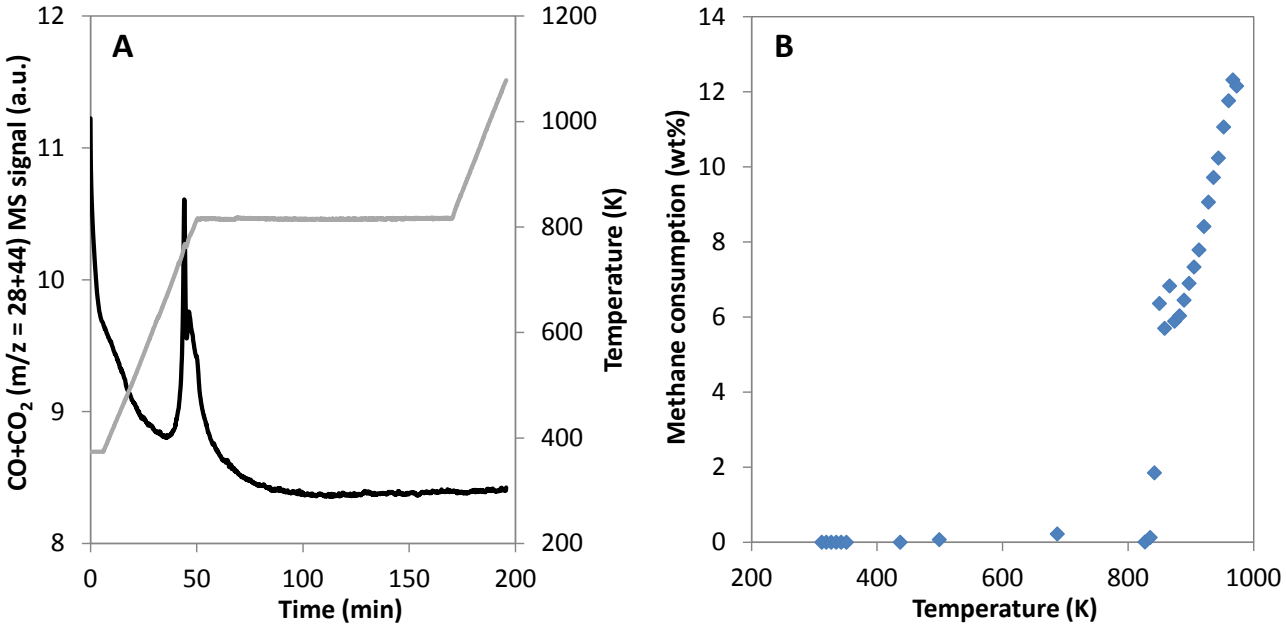
A
B
CO+CO2 (m/z = 28+44) MS signal (a.u.)
Temperature (K)
Time (min)
Methane consumption (wt%)
Temperature (K)

Figure 5.

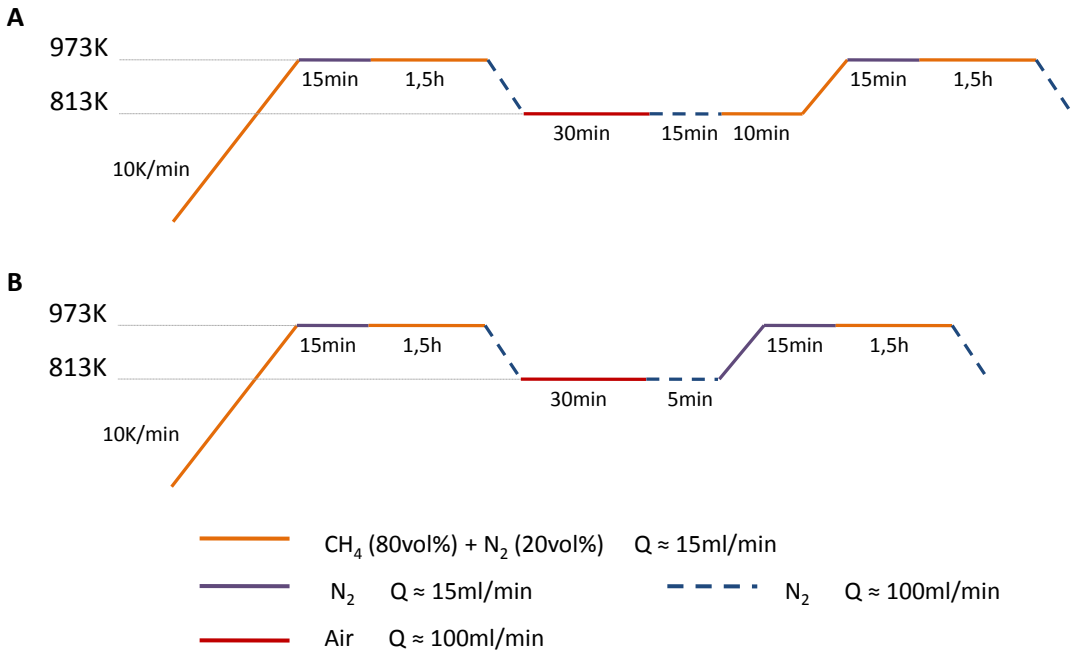
A
973K
813K
10K/min
15min
1,5h
30min
15min
10min
15min
1,5h
B
973K
813K
10K/min
15min
1,5h
30min
5min
15min
1,5h
CH4 (80vol%) + N2 (20vol%) Q ≈ 15ml/min
N2 Q ≈ 15ml/min
N2 Q ≈ 100ml/min
Air Q ≈ 100ml/min

Figure 6.

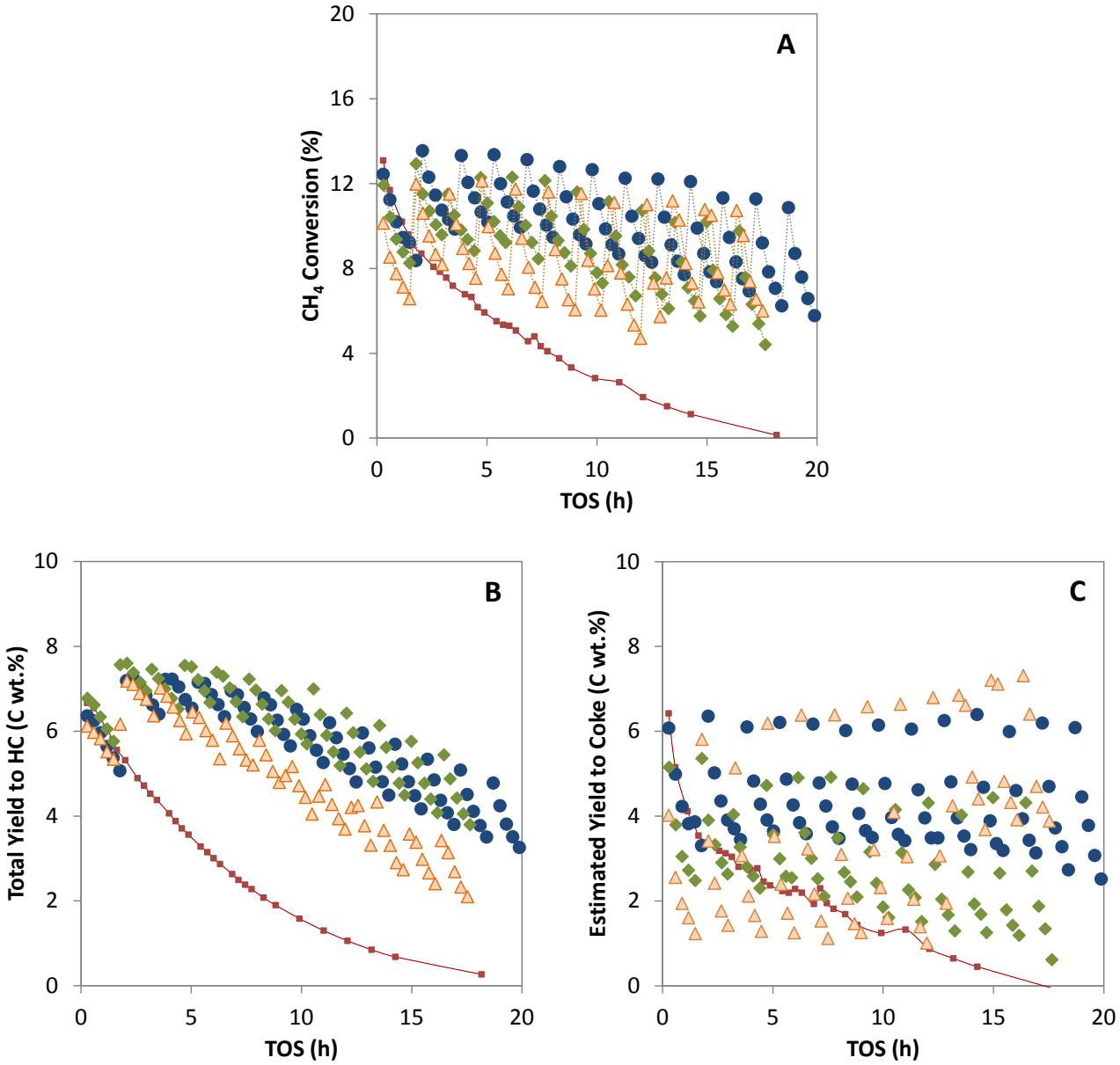
A
CH_4 Conversion (%)
TOS (h)
B
Total Yield to HC (C wt.%)
TOS (h)
C
Estimated Yield to Coke (C wt.%)
TOS (h)

Figure 7.

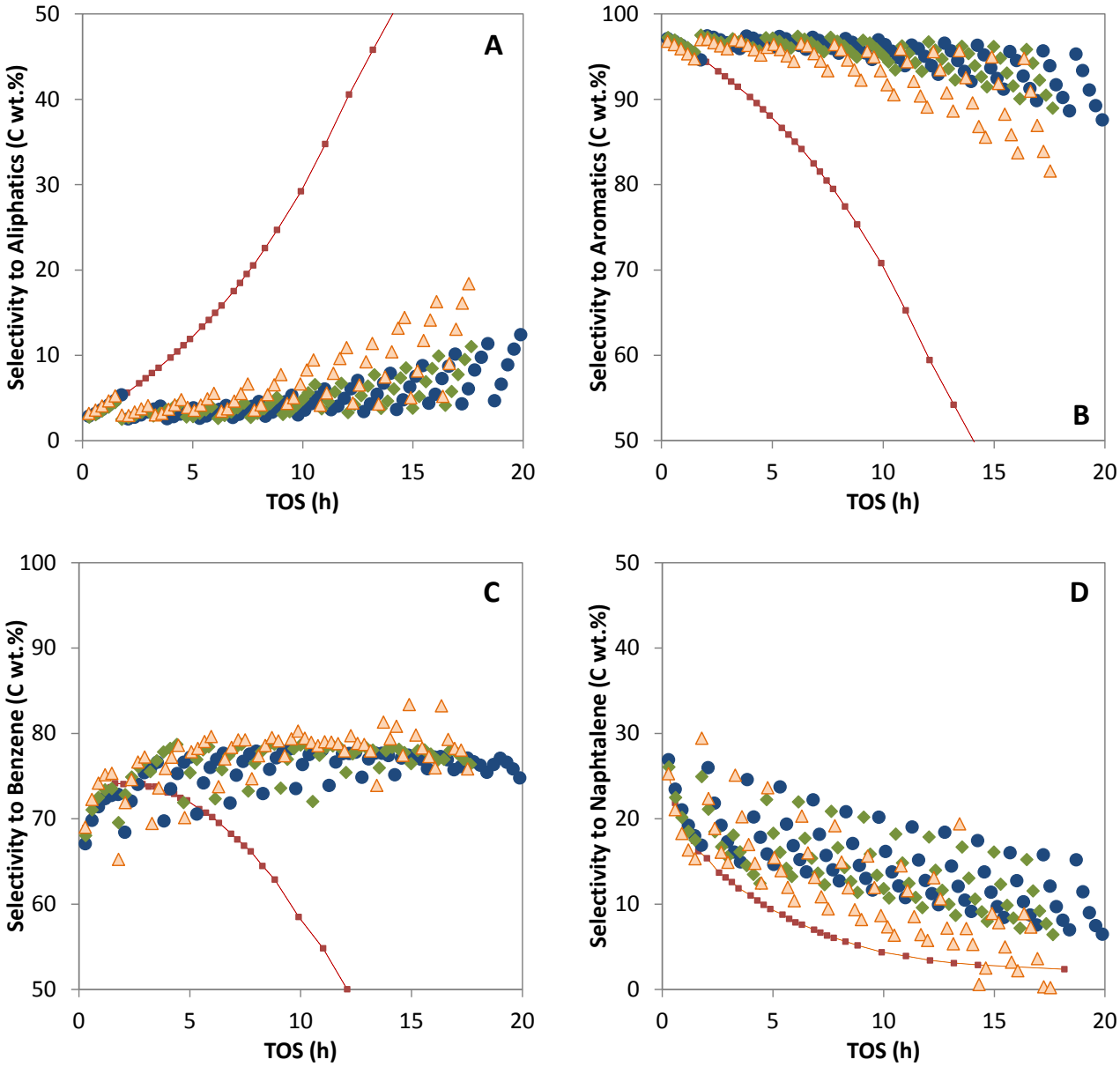
A
Selectivity to Aliphatics (C wt.%)
TOS (h)
B
Selectivity to Aromatics (C wt.%)
TOS (h)
C
Selectivity to Benzene (C wt.%)
TOS (h)
D
Selectivity to Naphtalene (C wt.%)
TOS (h)

Figure 8.

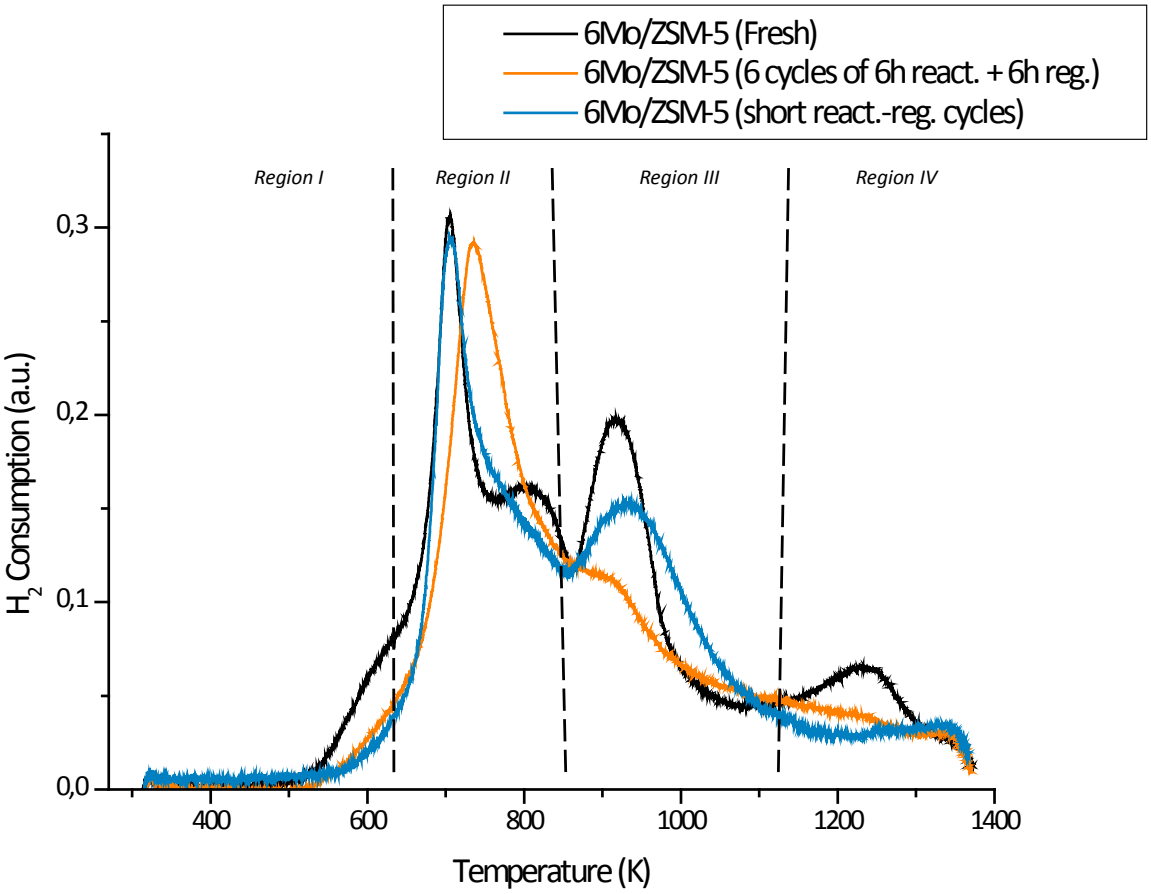
6Mo/ZSM-5 (Fresh)
6Mo/ZSM-5 (6 cycles of 6h react. + 6h reg.)
6Mo/ZSM-5 (short react.-reg. cycles)
Region I
Region II
Region III
Region IV
H2 Consumption (a.u.)
0,0
0,1
0,2
0,3
400
600
800
1000
1200
1400
Temperature (K)

Figure 9.

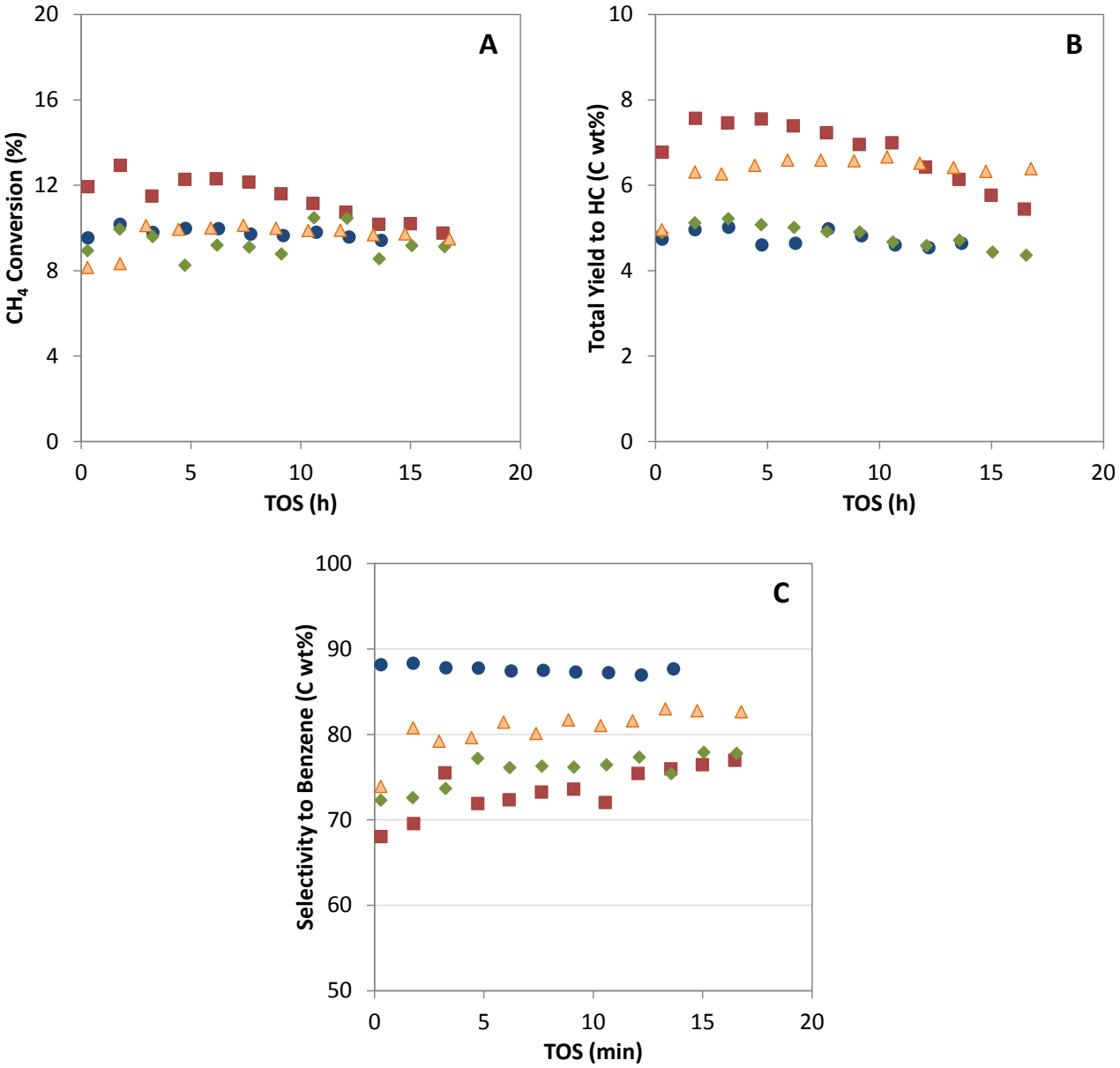
A
CH_4 Conversion (%)
TOS (h)
B
Total Yield to HC (C wt%)
TOS (h)
C
Selectivity to Benzene (C wt%)
TOS (min)

Table 1. Chemical composition and textural properties of Mo/ZSM-5 before and after being used as catalysts for MDA.

Sample	ICP			S_{BET}	S_{micro}	V_{micro}
	Si/Al	Mo/Al	wt% Mo	(m^2/g)	(m^2/g)	(cm^3/g)
ZSM-5	10.0	---	---	368	355	0.169
Mo/ZSM-5						
- Fresh	10.2	0.46	5.7	270	257	0.124
- After 6 cycles of 6 h react. + 6 h cal.	8.3	0.49	6.3	228	208	0.103
- After short react-reg. cycles(21 vol.% O_2)	9.6	0.49	6.3	232	213	0.104
- After short react-reg. cycles(10 vol.% O_2)	9.1	0.52	6.7	253	227	0.113
- After short react-reg. cycles without carburation	9.3	0.42	5.7	226	204	0.102

Table 2. Acidic properties of Mo/ZSM-5 before and after being used as catalysts for MDA.

Sample	Brønsted Acidity (mmol Py/g)				Lewis Acidity (mmol Py/g)		
	T=523K	T=623K	T=673K	B673/B523	T=523K	T=623K	T=673K
ZSM-5	0.564	0.368	0.241	0.43	0.007	0.000	0.000
Mo/ZSM-5							
- Fresh	0.213	0.121	0.107	0.50	0.023	0.014	0.003
- After 6 cycles of 6 h react. + 6 h cal.	0.080	0.039	0.020	0.25	0.029	0.015	0.005
- After short react-reg. cycles(21 vol.% O_2)	0.046	0.030	0.009	0.19	0.011	0.013	0.002
- After short react-reg. cycles(10 vol.% O_2)	0.060	0.044	0.024	0.40	0.028	0.033	0.022
- After short react-reg. cycles without carburation	0.037	0.017	0.006	0.17	0.019	0.014	0.011

Table 3. Benzene productivity (g benzene/kg cat·h) obtained with different reaction protocols and different TOS periods on Mo/ZSM-5

Reaction time on stream (TOS)	6.0	12.0	18.0
Single conventional run	72.6	48.9	33.8
1,5 h Reaction-0,5 h Regeneration	112.8	108.6	96.7

Table 4. Chemical composition and textural properties of Mo/IM-5, Mo/TNU-9 and Mo/MCM-22 before and after being used as catalysts for MDA.

Sample	ICP			S_{BET}	S_{micro}	V_{micro}
	Si/Al	Mo/Al	wt% Mo	(m^2/g)	(m^2/g)	(cm^3/g)
IM-5	12.7	---	---	339	323	0.158
Mo/IM-5						
- Fresh	12.4	0.6	6.2	300	285	0.140
- After short react-reg. cycles	10.5	0.6	6.3	239	225	0.110
TNU-9	13.5	---	---	394	379	0.186
Mo/TNU-9						
- Fresh	12.4	0.6	6.3	300	285	0.140
- After short react-reg. cycles	11.8	0.6	6.1	279	263	0.129
MCM-22	9.5	---	---	495	402	0.197
Mo/MCM-22						
- Fresh	9.3	0.5	5.8	374	300	0.143
- After short react-reg. cycles	8.8	0.4	6.1	295	218	0.106

Table 5. Acidic properties of Mo/IM-5, Mo/TNU-9 and Mo/MCM-22 before and after being used as catalysts for MDA

Sample	Brønsted Acidity (mmol Py/g)				Lewis Acidity (mmol Py/g)		
	T=523K	T=623K	T=673K	B673/B523	T=523K	T=623K	T=673K
IM-5	0.338	0.254	0.135	0.40	0.064	0.055	0.041
Mo/IM-5							
- Fresh	0.113	0.097	0.038	0.34	0.026	0.029	0.022
- After short react-reg. cycles	0.103	0.057	0.034	0.33	0.036	0.023	0.021
TNU-9	0.347	0.253	0.189	0.55	0.056	0.053	0.053
Mo/TNU-9							
- Fresh	0.112	0.064	0.034	0.31	0.031	0.021	0.011
- After short react-reg. cycles	0.099	0.044	0.030	0.31	0.028	0.013	0.007
MCM-22	0.180	0.140	0.103	0.57	0.030	0.042	0.054
Mo/MCM-22							
- Fresh	0.108	0.079	0.030	0.28	0.046	0.044	0.037
- After short react-reg. cycles	0.064	0.024	0.015	0.24	0.026	0.016	0.006